

CPSF6-RAR γ interacts with histone deacetylase 3 to promote myeloid transformation in RARG-fusion acute myeloid leukemia

Received: 28 November 2023

Accepted: 21 November 2024

Published online: 13 January 2025



Tianhui Liu^{1,2,5}, Tanzhen Wang^{1,2,5}, Lijuan Qi^{1,2,5}, Yujie Liu^{1,2,5}, Meng Shan^{1,2}, Fuqiang Wang³, Yanglan Fang^{1,2}, Sining Liu^{1,2}, Lijun Wen^{1,4}, Suning Chen^{1,4}✉, Depei Wu^{1,2}✉ & Yang Xu^{1,2}✉

Acute myeloid leukemia (AML) with retinoic acid receptor gamma (*RARG*) fusions, which exhibits clinical features resembling acute promyelocytic leukemia (APL), has been identified as a new subtype with poor clinical outcomes. The underlying mechanism of *RARG*-fusion leukemia remains poorly understood, and needs to be explored urgently to instruct developing effective therapeutic strategies. Here, using the most prevalent *RARG* fusion, *CPSF6-RARG* (*CR*), as a representative, we reveal that the *CR* fusion, enhances the expansion of myeloid progenitors, impairs their maturation and synergizes with *RAS* mutations to drive more aggressive myeloid malignancies. Mechanistically, *CR* fusion interacts with histone deacetylase 3 (HDAC3) to suppress expression of genes associated with myeloid differentiation including the myeloid transcription factor PU.1. Disrupting *CR*-HDAC3 interaction, restores PU.1 expression and myeloid differentiation. Furthermore, HDAC inhibitors effectively suppress *CR*-driven leukemia in vitro and in vivo. Hence, our data reveals the molecular bases of oncogenic *CR* fusion and provides a potential therapeutic approach against AML with *CR* fusion.

The success of treating acute promyelocytic leukemia (APL) with all-trans retinoic acid (ATRA) and arsenic trioxide (ATO) has revolutionized cancer therapy by inducing the differentiation of immature cancer cells. Differentiation therapy has greatly benefited patients with *PML-RARA* fusion, resulting in an overall survival rate of more than 95%^{1–3}. APL harbors a t(15:17) chromosomal translocation that results in the fusion of the *PML* gene to retinoic acid receptor alpha (*RARA*). While the *PML-RARA* fusion drives the pathogenesis of APL, it also determines sensitivity to ATRA or ATO^{4–6}. In addition to the *PML* gene, *RAR* genes are frequently

translocated to other regions in the genome, resulting in different *RAR* fusion genes in various subcategories of APL-like myeloid leukemias^{7–10}. Despite sharing similar clinical features with t(15:17) translocation, APL-like myeloid leukemias are not sensitive to ATRA and/or ATO treatment and usually have a poor outcome^{11–13}. In addition, the molecular mechanisms of pathogenesis are largely unknown, and the effective therapeutic strategies needs to be developed urgently.

Retinoic acid receptor gamma (RAR γ) is a key regulator of normal blood cell development. It regulates hematopoietic stem cell (HSC) self-

¹National Clinical Research Center for Hematologic Diseases, Jiangsu Institute of Hematology, The First Affiliated Hospital of Soochow University, Suzhou 215006, China. ²Institute of Blood and Marrow Transplantation, Collaborative Innovation Center of Hematology, Soochow University, Suzhou 215000, China. ³Suzhou Institute of Systems Medicine, Chinese Academy of Medical Sciences & Peking Union Medical College, Suzhou 215123, China. ⁴Key Laboratory of Thrombosis and Hemostasis of Ministry of Health, Suzhou 215006, China. ⁵These authors contributed equally: Tianhui Liu, Tanzhen Wang, Lijuan Qi, Yujie Liu. ✉e-mail: chensuning@suda.edu.cn; drwudepei@163.com; yangxu@suda.edu.cn

renewal through Notch1 signaling^{14–16}. Interrupting mutations in the *RARG* gene impair normal hematopoiesis and predispose to the development of myeloid malignancies¹⁷. Recently, *RARG* rearrangements were frequently reported in myeloid malignancies with the advancement and application of high-throughput sequencing technologies at diagnosis^{18–25}. A worldwide study revealed that patients with *RARG* fusions formed a unique group with morphology, immunophenotype, transcriptional landscape and other features similar to those of APL patients with *PML-RARA*²⁶. However, these patients are insensitive to ATRA or ATO treatment^{27–29}. Patients carrying *RARG* fusions have worse clinical outcomes, with a 2-year relapse rate of 68.7% and a survival rate of 33.5%²⁶.

More than 6 different types of *RARG* fusions have been reported, including *CPSF6-RARG* (*CR*)^{7,18–20,30}, *NUP98-RARG*^{21,31,32}, *HNRNPc-RARG*^{25,33}, *HNRNPm-RARG*²², *PML-RARG*³⁴ and *NPM1-RARG*²⁸. *CR* and *NUP98-RARG* are the 2 most frequently observed fusions in patients, with incidence of 41% and 32%, respectively²⁶. Interestingly, patients with *RARG* fusions frequently harbor concurrent mutations in *RAS* family genes, such as *NRAS*^{G12D} or *KRAS*^{Q61H}, suggesting possible cooperation between the 2 genetic events in leukemogenesis. All *RARG* fusions retain conserved DNA-binding domains, which play essential roles in transcriptional regulation³⁵. *RARG* exerts dual roles of transcription repression and activation, while it inhibits transcription by recruiting corepressors and histone deacetylases (HDACs)^{35,36}. The fusion of *RARG* to different partner genes may change the genomic occupancy and function of transcriptional regulation by recruiting different repressors such as HDACs, which may contribute to the development of disease.

Here, we demonstrate that *CR* fusion impairs myeloid development in *CR* knock-in mice and human CD34⁺ cell xenograft models. *CR* fusion interacts with HDAC3 to suppress gene expression and cooperates with *NRAS*^{G12D} or *KRAS*^{Q61H} to drive more advanced myeloid malignancies. Disrupting the *CR*-HDAC3 interaction selectively suppresses *CR* fusion-leukemia, which could be a potential therapeutic choice.

Results

CR fusions promote myeloid expansion in mice

To evaluate the effect of *CR* fusion on hematopoiesis, we generated conditional knock-in mouse models with two transcripts (*CRL* and *CRS*) reported in our previous study¹⁸ (Supplementary Fig. 1a). Conditional knock-in mice were bred with *Vav-Cre* mice to selectively express *CR* fusion proteins in hematopoietic cells (Fig. 1a, Supplementary Fig. 1b). All the Mice were genotyped by genomic polymerase chain reaction (PCR), and the expression of transgenes in bone marrow (BM) cells was confirmed by reverse transcription PCR (RT-PCR), immunoblotting and flow cytometry (Supplementary Fig. 1c–f). The expression levels of *CR* fusions in the knock-in mice were comparable to those observed in *CR*-AML patients (Supplementary Fig. 1g).

Vav-CRL and *Vav-CRS* mice exhibited increased white blood cells (WBCs) and decreased hemoglobin (Hgb) and platelets (PLTs) in peripheral blood (PB) at 12 months of age (Fig. 1b). The expression of *CR* fusions significantly increased the population of myeloid cells (Mac1⁺Gr1⁺), and decreased the proportion of erythrocytes (Ter119⁺) and B cells (B220⁺), but had less impact on T cells (CD3⁺) in the BM and PB (Fig. 1c and Supplementary Fig. 1h, i). We next examined the more primitive populations by flow cytometry. Mice with *CR* expression had more myeloid progenitors (LK, Lineage[−]IL7R[−]sca-1⁺Kit⁺), which is likely due to the expansion of common myeloid progenitor cells (CMPs) and granulocyte-monocyte progenitor cells (GMPs) in the BM (Fig. 1d). Interestingly, *CR* fusions strikingly increased the populations of Lin[−]Sca1⁺cKit⁺ (LSK) cells, long-term HSCs (LT-HSCs) and short-term HSCs (ST-HSCs, Fig. 1e). We also observed mild splenomegaly (Supplementary Fig. 1j), leukocytosis of neutrophilic and monocytic cells in the BM (Fig. 1f, g) and infiltration of leukocytes in the spleen and liver (Supplementary Fig. 1k). BM cells from knockin mice were then isolated for colony-forming assays. The results showed that BM cells from

either *Vav-CRL* or *Vav-CRS* mice could generate more myeloid colonies than those from WT mice (Supplementary Fig. 1l). These data suggested that *CR* fusions drive the proliferation and expansion of HSPCs and enhance myeloid differentiation.

To determine the effect of *CR* fusions on the stemness of HSPCs, we performed competitive repopulation assays (Fig. 1h). Wild-type (WT) competitor (CD45.1⁺) BM cells were mixed with CD45.2 WT, *Vav-CRL* or *Vav-CRS* BM cells at a 1:1 ratio. Cells were retro-orbitally injected into lethally irradiated recipients (CD45.1 mice). Recipients with *Vav-CRL* and *Vav-CRS* showed increased proportions of chimerism (Supplementary Fig. 1m) and chimeric tdTomato⁺ cells (Supplementary Fig. 1n). Notably, the proportion of myeloid cells derived from *Vav-CRL* and *Vav-CRS* donors was significantly higher than that from WT donors, in primary and secondary transplantation (Fig. 1i, j), suggesting enhanced self-renewal and repopulating capability of myeloid progenitors and in HSCs.

To further reveal the effect of *CR* fusions on the myeloid lineage, we crossed *CR* conditional knock-in mouse models with *LysM-Cre* mice to achieve myeloid-specific expression of *CR* fusions (Supplementary Fig. 2a). Consistent with the phenotype of *Vav-CR* (*Vav-CRL* and *Vav-CRS*) mice, *LysM-CRL* and *LysM-CRS* mice showed increased neutrophils in the PB (Supplementary Fig. 2b), and increased proportions of myeloid cells, including immature myeloid cells (Mac1⁺c-kit^{low}) and GMPs, in the BM (Supplementary Fig. 2c). BM Mac1⁺ and c-kit⁺ cells from WT, *LysM-CRL* or *LysM-CRS* mice were sorted and mixed at a 1:1 ratio to perform single-cell RNA sequencing (scRNA-seq). Nine subpopulations were clustered according to the transcription profiles (Supplementary Fig. 2d, e). Increased proportions of immature myeloid cells (IM) and granulocytes (G) were observed in cells from *LysM-CRL* or *LysM-CRS* mice compared with those from WT mice (Supplementary Fig. 2f). Gene set enriched analysis (GSEA) was performed in IM and G clusters. We discovered that several pathways were downregulated by *CR* fusions, including myeloid cell differentiation, migration and activation, and the pathway of regulation of the Mapk cascade was upregulated (Supplementary Fig. 2g, h). Genes critical for cell proliferation and differentiation, such as *Kras*, *Junb* and *Fos*, were upregulated. Transcription factors (TFs) for myeloid maturation, such as *Id2* and *Pu.1*, were downregulated (Supplementary Fig. 2i, j).

CR fusions disrupt myeloid differentiation of human HSPCs

To better understand the impact of *CR* fusions on human hematopoiesis, human CD34⁺ cells were enriched and transduced with lentivirus expressing *CRL*, *CRS*, or empty vector (Vec). GFP⁺ cells were sorted for the following in vitro assays, while total unsorted cells were transplanted into NCG (NOD/ShiLtJGpt-Prkdc^{em26cd52}/l2rg^{em26cd22}/Gpt) mice (Supplementary Fig. 3a). The protein levels of exogenous *CR* fusions in GFP⁺ cells, normalized by endogenous CPSF6, were comparable to those observed in *CR*-AML patients (Supplementary Fig. 3b). Compared to the Vec group, *CRL*- or *CRS*- expressing cells generated more myeloid and mixed-lineage colonies (Fig. 2a and Supplementary Fig. 3c). We then examined the colony-replating abilities of GFP⁺ cells. Both *CRL*- and *CRS*- expressing cells were able to generate colonies after 5 consecutive cultures, while no colonies were observed in the Vec group after 3 consecutive cultures (Fig. 2b), indicating an enhanced self-renewal capability of *CR*-expressing cells.

We next investigated the impact of *CR* fusions on myeloid differentiation. *CR*-expressing cells cultured in medium¹⁰ designed to promote myeloid cell development exhibited intensive proliferative capabilities (Fig. 2c and Supplementary Fig. 3d). These proliferative cells were composed of a large proportion of immature myeloid cells (CD34⁺CD33⁺) and fewer mature cells (CD66⁺CD33⁺, Fig. 2d and Supplementary Fig. 3e). Morphology analysis showed that the majority of cells were arrested at the myelocytic or promyelocytic stage in the *CR*-expressing groups (Fig. 2e).

To analyze the effect of *CR* on human hematopoietic cells in vivo, *CR*- or Vec- transduced cells were tibia injected into sub-lethal NCG

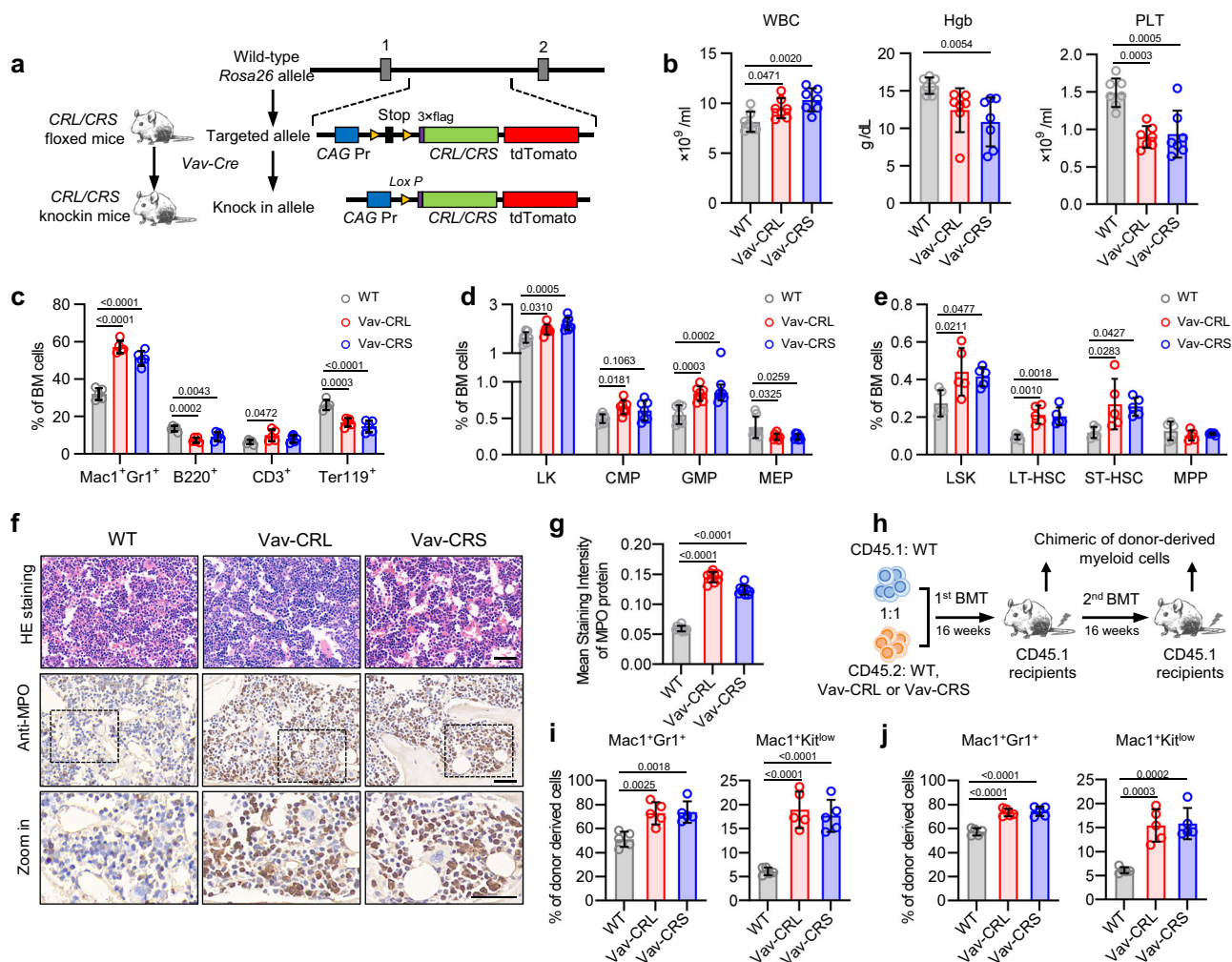


Fig. 1 | CR fusions promote myeloid expansion in knock-in mice. a Strategy design of *CRL* or *CRS* conditional knock-in mice. **b** Complete blood count (CBC) of peripheral blood (PB) white blood cells (WBCs), hemoglobin (Hgb) and platelets (PLTs) in 12-month-old mice with the indicated genotypes. *n* = 7 mice/group. **c–e** Flow cytometry quantification of BM lineage cells (**c** *n* = 5 mice/group), myeloid progenitors (**d** *n* = 7 mice/group), and HSPCs (**e** *n* = 5 mice/group) in WT (grey colour), Vav-CRL (red colour) and Vav-CRS (blue colour) mice. Mac1⁺Gr1⁺, myeloid cells; B220⁺, B cells; CD3⁺, T cells; Ter119⁺, erythrocytes; LK, myeloid progenitors (Lin⁺IL7R⁺sca-1⁺kit⁺); CMP, common myeloid progenitor (Lin⁺IL7R⁺sca-1⁺kit⁺CD34⁺CD16/32⁺); GMP, granulocyte-monocyte progenitor (Lin⁺IL7R⁺sca-1⁺kit⁺CD34⁺CD16/32⁺); MEP, megakaryocyte-erythroid progenitor (Lin⁺IL7R⁺sca-1⁺kit⁺CD34⁺CD16/32⁺); LSK (Lin⁺sca-1⁺kit⁺); LT-HSC, long-term hematopoietic stem cell (Lin⁺sca-1⁺kit⁺CD150⁺CD48⁺); ST-HSC, short-term hematopoietic stem cell (Lin⁺sca-1⁺kit⁺CD150⁺CD48⁺). MPP, multi-potent progenitor

(Lin⁺sca-1⁺kit⁺CD150⁺CD48⁺). **f** Representative hematoxylin and eosin (H&E) staining and immunohistochemistry of BM sections, showing the expansion of myeloid cells. Scale bars, 100 μ m. All images are representative of 5 mice/group. **g** Statistically analysis of the mean staining intensity of MPO protein from BM sections of WT or Vav-CR mice by QuPath software (*n* = 9 mice/group). **h** Schematic of competitive BM repopulation assays and the secondary transplantation. **i–j** Frequencies of donor-derived myeloid cells and immature myeloid cells (Mac1⁺Kit^{low}) in the BM of primary (**i** *n* = 5 mice/group) and secondary (**j** *n* = 5 mice/group) recipients. Heterozygous mice were included in the experiments to mimic the clinical situation (**b–g**). All the data are shown as the mean \pm SD, statistical analysis was performed by two-tailed one-way ANOVA with Dunnett's multiple comparisons test (**b–e**, **g**, **i**, **j**). See also Supplementary Figs. 1, 2. Source data are provided as a Source Data file.

mice, and the engraftment of human cells was analyzed 3 months post transplantation (Supplementary Fig. 3f–h). Consistent with the data from *in vitro* assays, the proportions of myeloid cells and myeloid precursors were significantly elevated, while the proportion of granulocytes decreased (Fig. 2f). In addition, the expression of CR fusions expanded the stem and progenitor pools (Fig. 2g). Moreover, myeloid cell expansion induced by CR fusions led to a reduction in B lymphocytes, compared with the Vec group (Fig. 2h). Hence, CR fusions impair normal hematopoiesis and induce a pre-leukemic phenotype in both murine and human models.

CR cooperates with oncogenic *RAS* to drive myeloid malignancy

Given that *RAS* mutations are common concurrent mutations in CR fusion patients (Fig. 3a) and that mouse models with *RAS* mutations were readily available, we wanted to test the hypothesis that CR fusion

was able to synergize with oncogenic *RAS* to promote leukemogenesis. We established a viral mouse model by expressing oncogenic *RAS* in CR fusions HSPCs. C-kit⁺ cells from WT or Vav-CR mice were enriched and subsequently transduced with virus expressing Vec, *NRAS*^{G12D} or *KRAS*^{Q61H} mutation (Supplementary Fig. 4a, b). Cells were then transplanted to sublethally irradiated recipients (Fig. 3b). Remarkably, *NRAS*^{G12D} alone (WT/N) induced disease-related death with a median survival date of 150 days after BM transplantation (BMT). CR significantly accelerated leukemia progression, while CR/*NRAS*^{G12D} (CR/N, CRL/N or CRS/N) mice died of leukemia within 110 days, which was significantly earlier than WT/N mice (Fig. 3c, top panel). Similar results were obtained in CR/*KRAS*^{Q61H} mice (Fig. 3c, bottom panel). No WT/*KRAS*^{Q61H} (WT/K) mice died of leukemia during the observation period (Fig. 3c, bottom panel). The double mutant mice had leukocytosis, anemia, thrombocytopenia (Supplementary Fig. 4c, d) and increased

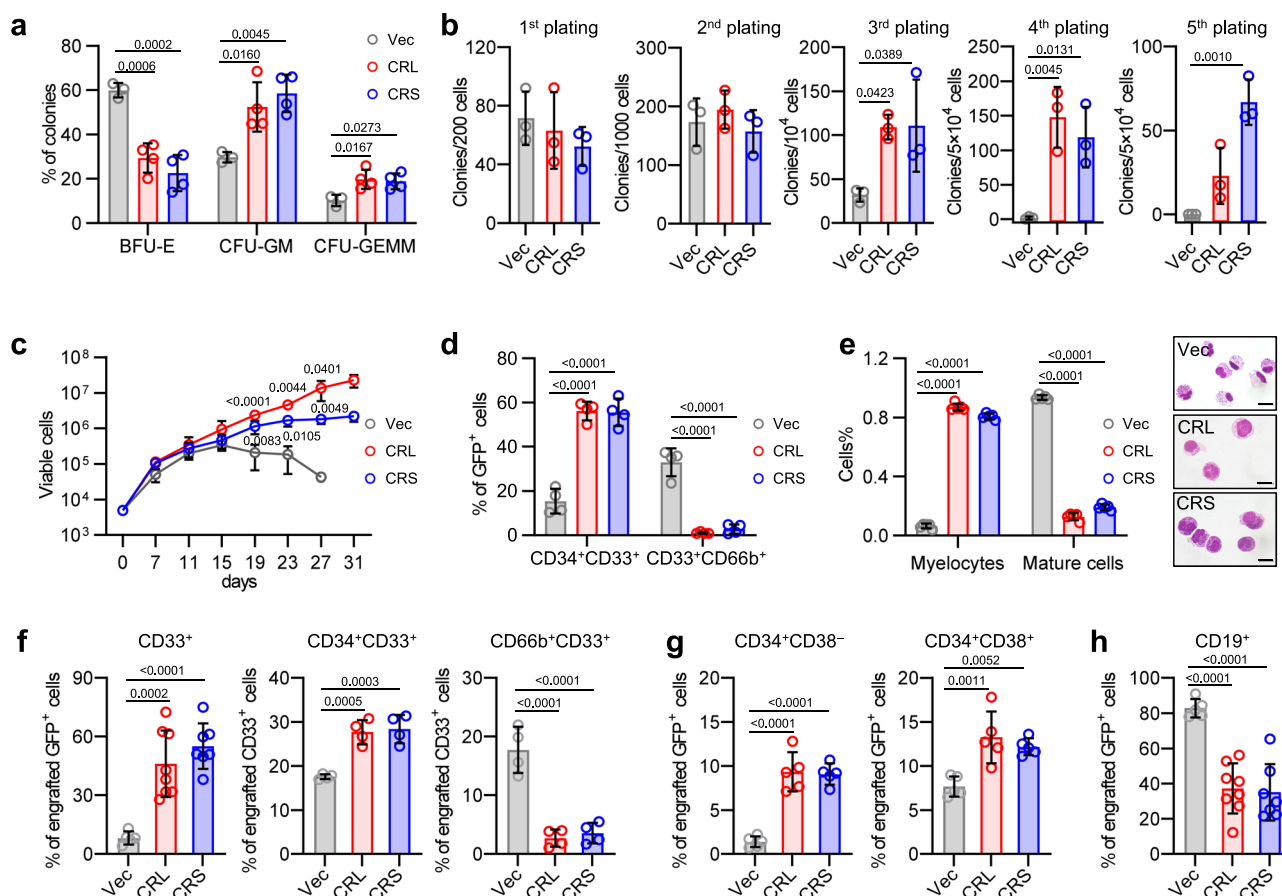


Fig. 2 | CR fusions disrupt myeloid differentiation of human HSPCs. **a** Colony-forming assays of human CD34⁺ cells transduced with the indicated genes in the H4435 methylcellulose medium. *n* = 3 independent donors in *n* = 3 independent experiments (Vec group) and in *n* = 4 independent experiments (CRL and CRS groups). **b** Serial colony-forming assays of the cells used in **a**. *n* = 3 independent donors in *n* = 3 independent experiments. **c** The growth curves of human CD34⁺ cells ectopically expressing with the indicated genes in myeloid differentiation medium. Statistical analysis was performed by unpaired two-tailed Student's *t*-test. **d** Flow cytometry quantification of myeloid precursors (CD34⁺CD33⁺) and myeloid mature cells (CD66b⁺CD33⁺) in myeloid differentiation medium on day 14. **e** Statistical results and representative images of morphologic myelocytes and

myeloid mature cells. Scale bars, 5 μ m. *n* = 2 independent donors in *n* = 4 independent experiments (**c–e**). **f–h** The frequencies of myeloid cells (**f**), HSPCs (**g**), and B cells (**h**) in engrafted GFP⁺ cells in xenograft models. CD33⁺, myeloid cells (Vec, *n* = 5 mice; CRL, *n* = 8 mice; CRS, *n* = 7 mice); CD34⁺CD33⁺, myeloid precursors; CD33⁺CD66b⁺, granulocytes (*n* = 4 mice/group); CD34⁺CD38⁺, primitive stem cell populations; CD34⁺CD38⁺, committed progenitors (*n* = 5 mice/group); CD19⁺, B cells (Vec, *n* = 5 mice; CRL, *n* = 8 mice; CRS, *n* = 7 mice). All the data are shown as the mean \pm SD. Statistical analysis was performed by two-tailed one-way ANOVA with Dunnett's multiple comparisons test between the CR group and Vec group (**a**, **b**, **d–h**). See also Supplementary Fig. 3. Source data are provided as a Source Data file.

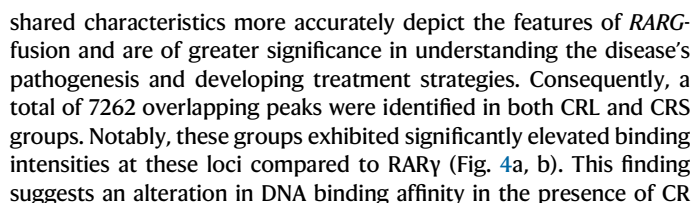
GFP⁺ cells (cells expressing RAS mutation) in BM and spleen (Fig. 3d). The GFP⁺ leukemic cells predominantly consist of Mac1⁺Gr1⁺ cells (Fig. 3e and Supplementary Fig. 4e, f). CR/N mice exhibited massive hepatosplenomegaly (Fig. 3f). Pathological examination confirmed robust blasts infiltration in the BM, spleen and liver (Fig. 3g and Supplementary Fig. 4g). Increased myeloblasts were observed in BM cytopspins by Wright-Giemsa staining (Fig. 3g). It is noted that the disease burden was more severe in CR/N mice than in WT/N mice, indicating a more profound lesion of hematopoiesis in the double mutant groups. Collectively, these data showed that CR fusions enhanced *NRAS*^{G12D} or *KRAS*^{Q61H} induced leukemogenesis in vivo.

To reveal the impact of CR fusions on the transformation of myeloid malignancies driven by CR fusions and *NRAS*^{G12D}, we performed scRNA-seq analysis in Mac1⁺ and Kit⁺ cells (mixed at a 1:1 ratio) isolated from WT/V, CR/V, WT/N and CR/N mice. Seven transcriptionally distinct cell clusters were identified (Fig. 3h and Supplementary Fig. 4h). Leukemic cells exclusively present in the *NRAS*^{G12D} groups were characterized based on the expression of human *NRAS* (Fig. 3i), and subsequently classified into six distinct subsets (Fig. 3j). Compared to WT/N group, CRL/N and CRS/N groups showed a higher proportions of subpopulations C2, C3 and C4 (Fig. 3k). Comparative

analysis of transcriptional profiles between CR/N and WT/N in these subsets revealed significant enrichment of myeloid cell development, Hdac3 targets, HSC signatures, fatty acid metabolism and TNF- α /NF- κ B signaling pathway within both the CRL/N and CRS/N groups (Fig. 3l, m). These findings suggest an altered myeloid differentiation and myeloid transformation in CR/N mice.

CR alters target profiles by increasing chromatin occupancy

As RAR γ regulates gene expression by direct DNA binding, we sought to address how CR fusions affect gene expression, which may disturb myeloid development and contribute to pre-leukemia transformation. We performed cleavage under targets and tagmentation sequencing (CUT&Tag-seq) on human CD34⁺ cells with consistent expression levels of flag-CRL, flag-CRS and flag-RAR γ using the flag antibody (Supplementary Fig. 5a). We found that CRL, CRS, and RAR γ exhibit strong binding signals on DNA (Supplementary Fig. 5b). Interestingly, we identified approximately 2-fold increase of peak numbers in the CRL and CRS groups compared to the RAR γ group (9005 peaks of CRL, 10306 peaks of CRS and 3696 peaks of RAR γ identified in CD34⁺ cells), suggesting increased DNA-binding sites for the CR fusions. While distinctions were observed between CRL and CRS, we propose that the

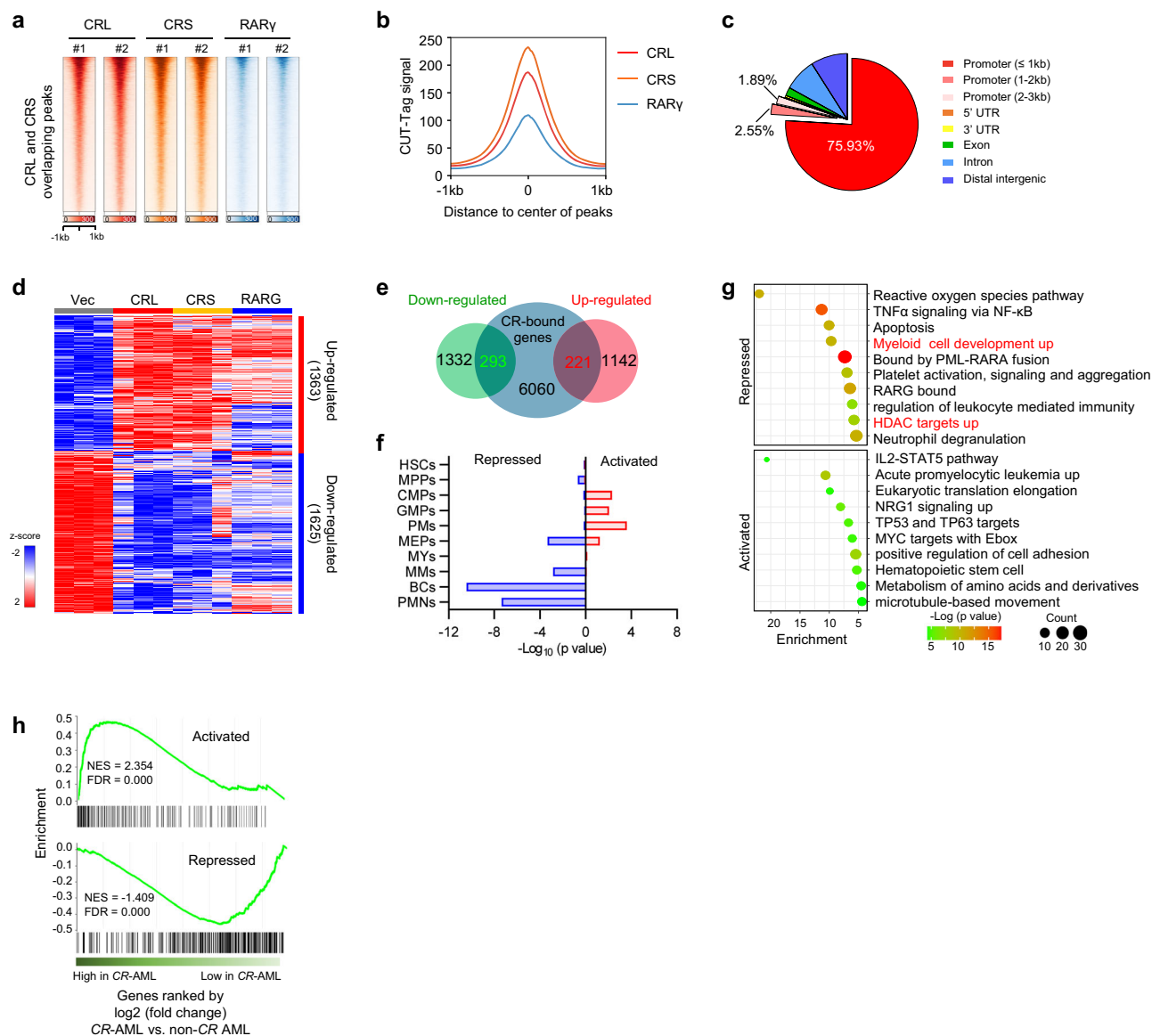


RNA sequence (RNA-seq) was performed in human CD34⁺ cells to analyze differentially expressed genes by *CRL*, *CRS* and *RARG* expression. We identified 1363 genes that were upregulated and 1625 genes

Fig. 3 | CR fusion cooperates with oncogenic *RAS* to drive myeloid malignancy.

a Diagram of concurrent mutations with *RARG* fusions in *RARG*-AML. **b** Schematic of the double mutation mouse model. **c** Survival curves of recipients transplanted with the indicated cells. Statistical analysis was performed by Log-rank test. **d** Flow cytometry analysis of GFP⁺ cells in the BM (CRS/N, *n* = 4 mice) and spleen of recipients. BM and spleen: WT groups, *n* = 5 mice/group; CRL/CRS groups, *n* = 6 mice/group. **e** Flow cytometry qualification the proportion of Mac1⁺Gr1⁺ cells among GFP⁺ cells in WT/N and CR/N mice. Spleen WT groups, *n* = 3 mice/group; other groups, *n* = 5 mice/group. **f** Representative pictures of spleen and statistical results of spleen and liver weight. *n* = 6 mice/group. **g** Representative H&E staining of BM, spleen and liver sections, and Wright-Giemsa staining of BM cytopspins of recipients. Scale bars, 100 μ m for tissue section and 5 μ m for BM cytopspins. The images are representative of 3 mice/group. **h** UMAP displaying seven distinct cell

populations in the BM cells of recipients, including hematopoietic stem cell/multipotent progenitor (HSC/MPP), common myeloid progenitor (CMP), granulocyte and monocyte progenitor (GMP), pro-monocyte (pro-mono), monocyte (mono), early differentiation stage granulocyte (early_GN), and late differentiation stage granulocyte (late_GN). **i** Leukemic cell population was defined by human *NRAS* expression. **j** The re-clustered leukemic cell subsets. **k** The proportion of leukemic subsets in WT/N and CR/N mice. **l–m** The enriched gene set enrichment analysis (GSEA) terms for CRL/N (**l**) and CRS/N (**m**), in comparison to WT/N, were identified within leukemia clusters C2 to C4. The *P*-value is calculated via two-tailed permutation test. All the data are shown as the mean \pm SD, statistical analysis was performed by two-tailed one-way ANOVA with Tukey's multiple comparisons test (**d–f**). See also Supplementary Fig. 4. Source data are provided as a Source Data file.

**Fig. 4 | CR fusion alters target gene profiles by increasing chromatin occupancy.**

a–b Heatmaps (**a**) and profiles (**b**) of CUT&Tag-seq signal intensities displaying loci clusters of overlapping peaks for CRL and CRS in human CD34⁺ cells. **c** Genome-wide distribution of overlapping peaks for CRL and CRS. **d** Heatmaps presenting the common differentially expressed genes of CRL and CRS identified by RNA-seq in human CD34⁺ cells. **e** Venn diagram showing that overlapping genes were targets for CR fusions. **f** Enrichment analysis of activated and repressed genes using the gene sets specifically expressed in myeloid cells with 10 differentiation

stages. PMs, promyelocytes; MYs, myelocytes; MM, metamyelocytes; BCs, band cells; PMNs, polymorphonuclear cells. **g** Top enriched signatures in activated or repressed targets in human CD34⁺ cells expressing CRL or CRS. **h** Pre-ranked GSEA to examine the specificity of CR activated and repressed target genes using RNA-seq data from CR-AML and non-CR AML patients. The statistical significance of enrichment was determined by the two-tailed hypergeometric test (**f, g**). See also Supplementary Fig. 5. Source data are provided as a Source Data file.

that were downregulated in both the CRL and CRS groups compared to the Vec group ($\text{LogFC} \geq 1.0$, $P < 0.05$, Fig. 4d). Moreover, we observed that 61.0% of the upregulated genes and 72.9% of the down-regulated genes were commonly shared in the RARG group (Supplementary Fig. 5c), suggesting a pivotal role for the RAR γ segment of the CR fusion in its functionality.

To identify targets directly affected by CR fusions, we integrated the CUT&Tag-seq data and RNA-seq data of CD34⁺ cells and found 514 CR direct targets, including 221 activated genes and 293 repressed genes (Fig. 4e and Supplementary Data 1). We next investigated the myeloid development relevance of these two classes of CR targets by hypergeometric analysis with gene signatures for myeloid differentiation stages³⁷. We observed that CR-repressed targets tended to be correlated with mature myeloid progeny, including metamyelocytes (MMs), band cells (BCs) and polymorphonuclear neutrophils (PMNs, Fig. 4f). In agreement with this, we discovered that the repressed target genes were mainly involved in myeloid cell differentiation and HDAC targets (Fig. 4g). Furthermore, we examined the disease relevance of the two classes of CR target genes by conducting pre-ranked GSEA using RNA-seq data from 8 CR-AML and 113 non-CR AML patients²⁶. Our results revealed that the activated target genes were enriched among highly expressed genes in CR-AML, while repressed target genes showed down-regulation (Fig. 4h) when comparing CR-AML with non-CR AML. This suggests the specificity of both classes of CR target genes to CR-AML and their association with malignancy.

HDAC3 is indispensable for CR-driven myeloid aberrance

Given that CR-repressed targets were associated with myeloid development and the enrichment of HDAC targets, as depicted in Fig. 4g, we wondered whether these repressed target genes are co-regulated by HDACs. As HDACs are important components of the RAR transcriptional complex that inhibit transcription in AML^{38,39}, we examined the possibility of protein interaction between HDACs and CR fusions by immunoprecipitation (IP) assays. Interestingly, both CRL and CRS were able to recruit HDAC3 (Fig. 5a and Supplementary Fig. 6a, b), while a weak interaction was detected in the IP assay using HDAC1 or HDAC2 antibody (Supplementary Fig. 6c), indicating the predominant involvement of HDAC3 in the interaction with CR. We also confirmed the CR-HDAC3 interaction in CR patient-derived xenografts (Supplementary Fig. 6d). Hence, we performed CUT&Tag-seq using an HDAC3 antibody in CD34⁺ cells expressing the CR fusion to explore whether the DNA occupancy of the CR fusion overlaps with that of HDAC3. Notably, 31.7% CRL peaks and 33.9% CRS peaks were shared with HDAC3, respectively (Fig. 5b). Moreover, the CR-HDAC3 common peaks were predominantly located on gene promoters (Supplementary Fig. 6e), suggesting a potential cooperation to suppress gene expression by CR and HDAC3 at promoter of target genes. Furthermore, we observed an overall downregulation in the expression levels of CR-HDAC3 target genes in CD34-CRL or CD34-CRS cells compared to CD34-Vec cells (Supplementary Fig. 6f). In contrast, the target genes of CR showed no significant changes.

To further elucidate the transcriptional cooperation of the CR-HDAC3 complex, we employed an HDAC3 specific inhibitor RGFP966⁴⁰ and an HDAC class I inhibitor tucidinostat⁴¹. The interaction between CR and HDAC3 was disrupted by HDAC inhibitors (Supplementary Fig. 6g), leading to attenuated DNA binding at the co-occupancy sites of CR-HDAC3, while maintaining consistent binding intensities at regions bound by CR fusions without HDAC3, observed in both CD34-CRL and CD34-CRS cells (Fig. 5c and Supplementary Fig. 6h). Consistently, treatment with HDAC inhibitors or shRNAs abolished the growth advantage of HSPCs expressing the CR fusions (Supplementary Fig. 6i), reduced the colony-forming cells (Fig. 5d, e), and induced myeloid differentiation (Fig. 5f, g and Supplementary Fig. 6j). These

data suggest a cooperative role of HDAC3 in sustaining the proliferation and myeloid abnormalities induced in CR-leukemic cells.

CR-HDAC3 complex transcriptionally inhibit PU.1 expression

The above data suggest that CR-HDAC3 complex orchestrates a transcription program that may contribute to the development of myeloid disease. Specifically, we observed a significant reduction in the binding of CR fusion to promoters of genes related to myeloid development in the presence of HDAC inhibitors (Supplementary Fig. 7a), and a corresponding increase in the expression of these genes following HDAC3 knockdown (Supplementary Fig. 7b). The most notable change is evident in PU.1 (Fig. 5h, i), a crucial transcription factor for myeloid maturation³⁹, with significantly suppressed expression in CR-expressing CD34⁺ cells and knock-in mice (Supplementary Fig. 7c). Treatment with HDAC inhibitors or HDAC3 silencing alleviated the transcriptional repression of PU.1 by CR fusion (Fig. 5j), and increased the levels of histone H3 acetylation and the expression of PU.1 (Fig. 5k and Supplementary Fig. 7d).

We subsequently induced ectopic expression of PU.1 to test whether downregulation of PU.1 is responsible for the CR fusion-induced arrest in myeloid differentiation. Human CD34⁺ cells were transduced sequentially with virus expressing CR fusion and PU.1 (Supplementary Fig. 7e). Expression of PU.1 significantly impaired the colony-forming abilities induced by CR fusions (Supplementary Fig. 7f) and promoted myeloid maturation (Supplementary Fig. 7g, h). These results indicate that suppression of PU.1 is required for the aberrant myeloid differentiation and maturation caused by CR-HDAC3. Additionally, following treatment with HDAC inhibitors, we utilized shRNAs to suppress PU.1 expression and evaluate whether the reduction of PU.1 expression could attenuate the apoptosis induced by HDAC inhibitors in CR-AML cells (Supplementary Fig. 7i). The HL60 cell line, which serves as a representative model for APL research and facilitates various manipulations, was employed. The results demonstrated that knockdown of PU.1 significantly attenuated the apoptosis induced by HDAC inhibitors in CR-AML cells (Fig. 5l). These data together suggest that PU.1 was transcriptionally repressed by CR-HDAC3, which promotes the development of myeloid malignancy. Disrupting CR-HDAC3 interaction restores PU.1 expression and myeloid differentiation.

Given that the distinct clinical outcomes observed in RARG-fusion AML and APL^{1,26}, we sought to conduct comparative analyses on target genes and drug sensitivity between these two fusions to offer insights for clinical treatment. Using ChIP-seq data from NB4 cells³⁷ and CUT&Tag-seq data from human CD34⁺ cells expressing PML-RARA, we unexpectedly discovered that only 10.7% or 14.2% of CR target genes were overlapped with those of PML-RAR α (Supplementary Fig. 8a), indicating unique pathogenic molecular mechanisms for CR-fusion leukemia. It is widely recognized that the PML-RAR α protein can be degraded by ATRA, ATO, or their combination^{1,3}. We also examined the expression of the CR fusions under these treatments. However, neither ATRA nor ATO, or their combination, induce degradation of the CR fusion proteins (Supplementary Fig. 8b). As HDAC inhibitors induce apoptosis in APL cells^{42,43}, particularly those resistant to ATRA and ATO⁴⁰, we assessed the sensitivity of U937 and HL60 cells expressing PML-RARA or CR to HDAC inhibitors. HDAC inhibitors induced 30–40% apoptosis in control cells (U937 or HL60 cells transduced with empty vector) and cells expressing PML-RARA. Surprisingly, HDAC inhibitors elicit significant higher capability of apoptosis inducing effect in AML cells expressing CR, compared to those expressing PML-RARA (Supplementary Fig. 8c), suggesting that HDAC inhibitors could be a potent therapeutic option for CR-AML. The expression of PU.1 showed a significantly increase upon treatment with an HDAC class I inhibitor but not with an HDAC3-specific inhibitor or HDAC3 shRNAs in CD34⁺ cells expressing PML-RARA. (Supplementary Fig. 8d).

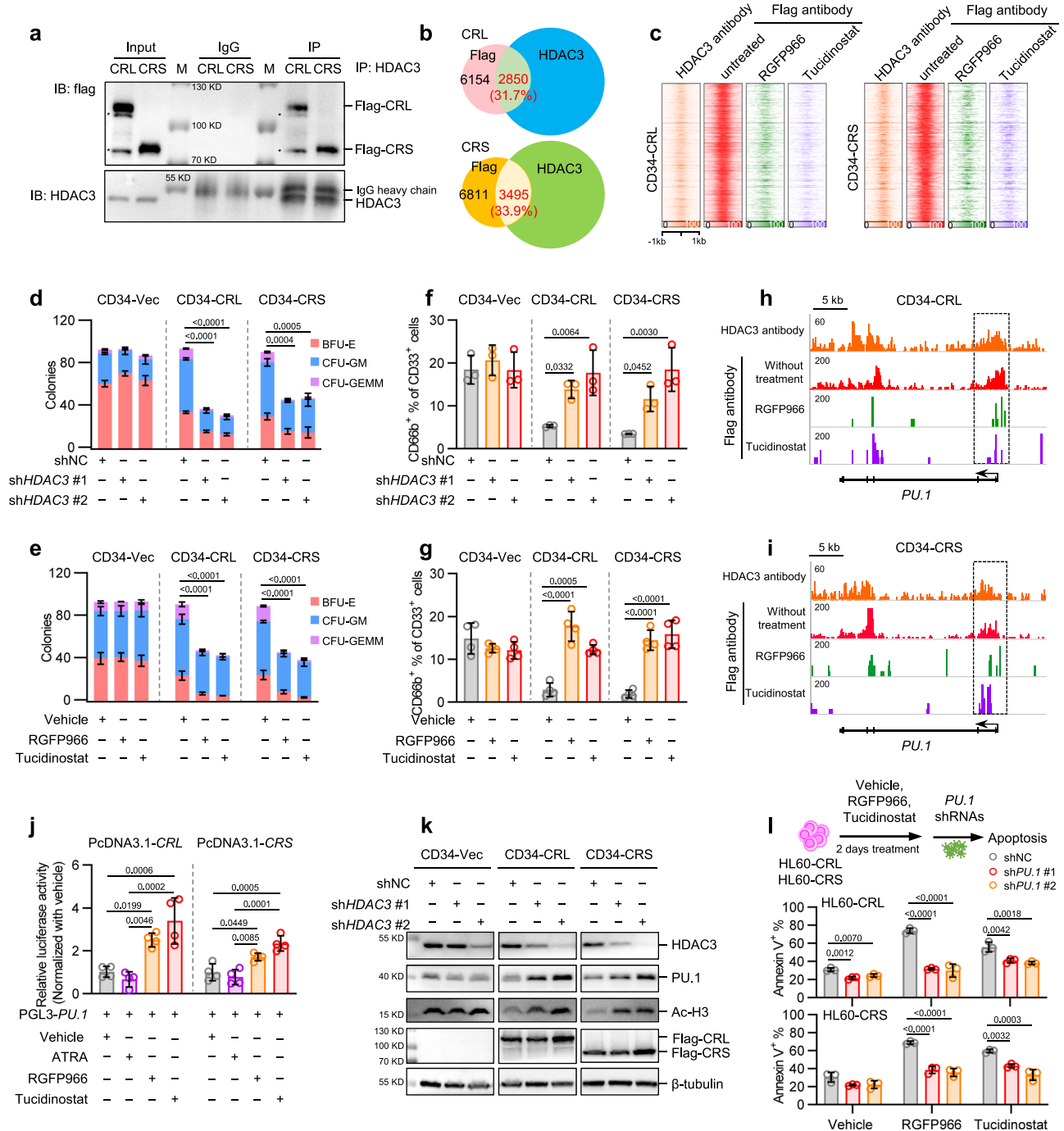


Fig. 5 | CR recruits HDAC3 to promote aberrant myeloid differentiation. a The interaction between CR fusions and HDAC3 in human CD34⁺ cells expressing *CR*. * indicate degraded flag-CRL proteins. M, markers. **b** Venn diagram displaying the shared peaks of CR fusions and HDAC3 in CD34⁺ cells expressing *CRL* (top panel) or *CRS* (bottom panel). **c** The heatmaps showing the signal intensities at DNA loci associated with common peaks of CR-HDAC3 in CD34-CR cells, both untreated and treated with RGFP966 or Tucidostat. **d–e** The colony-forming of CD34⁺ cells expressing *Vec*, *CRL* or *CRS* following silencing of *HDAC3* shRNAs (**d**) or treatment with HDAC inhibitors (**e**). *n* = 3 independent donors in *n* = 3 independent experiments. **f–g** Percentage of CD66⁺ cells assessed by flow cytometry in *CR*-expressing CD34⁺ cells after silencing of *HDAC3* shRNAs (**f**, *n* = 3 independent donors in *n* = 3 independent experiments) or treatment with HDAC inhibitors (**g**, *n* = 3

independent donors in *n* = 4 independent experiments). **h–i** HDAC inhibitors lead to significantly decreased CR binding at *PU.1* promoter in CD34-CRL (**h**) and CD34-CRS cells (**i**). **j** RGFP966 or tucidostat reversed the trans-repression of *PU.1*. *n* = 4 biological replicates. **k** The protein levels of PU.1 and acetylated histone H3 (Ac-H3) in CD34-CRL and CD34-CRS cells following silencing of *HDAC3* shRNAs. **l** Silencing of *PU.1* reduced the apoptosis induced by HDAC inhibitors in HL60-CR cells. *n* = 3 biological replicates. The data are shown as the mean ± SD, statistical analysis was performed by two-tailed one-way ANOVA with Dunnett's (**d–g**, **l**) or Tukey's (**j**) multiple comparisons test. The images are representative of three independent experiments from three healthy donors (**a**, **k**). See also Supplementary Figs. 6–8. Source data are provided as a Source Data file.

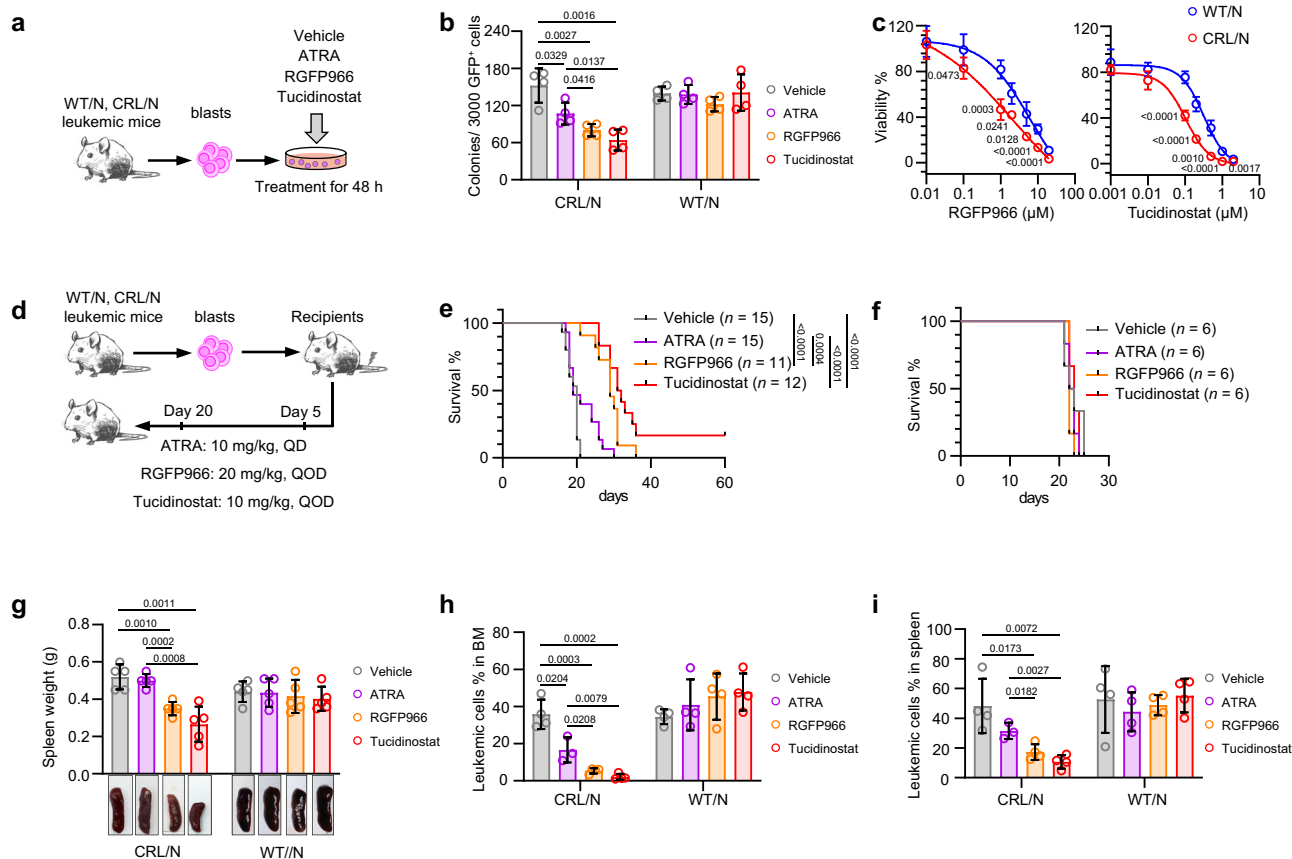


Fig. 6 | CR fusion-leukemia is sensitive to HDAC inhibitors. **a** Experimental design to determine the effects of HDAC inhibitors on blasts of CRL/N and WT/N mice in vitro. **b** Colony numbers generated by blasts from CRL/N and WT/N mice with indicated treatments. **c** The sensitivity of blasts from CRL/N and WT/N mice to HDAC inhibitors. $n = 4$ independent experiments using blasts from 2 CRL/N and 2 WT/N mice (**b**, **c**). **d** Experimental design to measure the effects of HDAC inhibitors on CRL/N and WT/N mice in vivo. **e–f** Survival curves of CRL/N mice (**e**) and WT/N mice (**f**) administered indicated regents. Three independent experiments were performed, with 3

to 5 mice per group in each experiment (**e**). Statistical analysis was performed by Log-rank test. **g** Representative pictures and quantification of spleens of CRL/N and WT/N mice after indicated treatments 20 days post-transplantation. $n = 5$ mice/group. **h–i** Frequency of leukemic cells in BM (**h**) and spleen (**i**) of CRL/N and WT/N mice administered indicated regents 20 days post-transplantation. CRL/N ATRA treatment, $n = 3$ mice; other groups, $n = 4$ mice/group. The data are shown as the mean \pm SD, statistical analysis was performed by two-tailed unpaired t test (**b–c**, **g–i**). See also Supplementary Fig. 9. Source data are provided as a Source Data file.

CR fusion-leukemia is sensitive to HDAC inhibitors

In order to further validate the efficacy of HDAC inhibitors in CR-AML, BM blasts from CRL/N mice or WT/N mice were treated with vehicle, ATRA, RGFP966 or tucidinostat for 48 h in vitro (Fig. 6a). Compared to vehicle or ATRA treatment, RGFP966 or tucidinostat treatment significantly impaired the colony-forming activities of leukemic cells from CRL/N mice (Fig. 6b), decreased blasts (Supplementary Fig. 9a), and increased apoptotic cells (Supplementary Fig. 9b), but did not exhibited significant therapeutic efficacy on WT/N leukemic cells (Fig. 6b). Subsequent drug sensitivity experiments also confirmed the enhanced sensitivity of CRL/N leukemic cells to HDAC inhibitors compared to WT/N leukemia cells (Fig. 6c).

We next evaluated the effects of ATRA or HDAC inhibitors in CRL/N mice and WT/N mice in vivo. Recipients were administered vehicle, ATRA, RGFP966 or tucidinostat for 15 days (Fig. 6d). Treatment with RGFP966 or tucidinostat significantly improved overall survival of CRL/N mice compared to vehicle- or ATRA-treated groups (Fig. 6e). However, the treatments did not lead to a significant improvement in the survival of WT/N mice (Fig. 6f). RGFP966 or tucidinostat treatment reduced hepatosplenomegaly (Fig. 6g and Supplementary Fig. 9c, d) and leukemia burden (Fig. 6h, i) in CRL/N mice. Consistent with our in vitro findings, administration of RGFP966 or tucidinostat eliminated blasts and leukemia-initiating cells⁴⁴ (Mac1⁺kit⁺) by inducing cell apoptosis in the BM and spleen (Supplementary Fig. 9e–g). Nevertheless, there were no significant differences were observed regarding hepatosplenomegaly,

tumor burden, as well as apoptosis of leukemic cells between the treatment groups and the control group in WT/N mice (Fig. 6g–i and Supplementary Fig. 9e–g). These data suggested that CR fusion-driven leukemia exhibits increased sensitivity to HDAC inhibitors, implying that HDAC inhibition may be a selective and effective therapeutic choice for leukemia patients with CR fusions.

Discussion

Retinoic acid signaling via ligand-activation of RARs plays crucial roles in embryo development^{15,45} and pathogenesis including cancers⁴⁶. *RARG* maintains the balance between the self-renewal and differentiation of HSCs^{14,16}. High levels of *RARG* expression have been reported in some carcinomas and are associated with increased cell proliferation, rapid tumor progression, and a poor prognosis⁴⁷. However, the roles of *RARG* fusions in the pathogenesis of hematopoietic malignancies remain unknown. In the present work, using the most prevalent *RARG* fusion-*CR* fusion as a representative, we de novo generated knock-in mouse models of *CR* fusions and provided compelling evidence that CR fusions impair myeloid differentiation by promoting the expansion of myeloid progenitor cells and enhancing their reconstructive ability. Consistent with data from genetic mouse models, CR fusions also suppress the maturation of human CD34⁺ cells, promote proliferation and increase colony-forming abilities. The phenotype induced by CR fusions were similar to that induced by *PML-RARA*, which was consistent with the clinic diagnosis of APL-like disease.

It is well recognized that the chimeric gene *PML-RARA* is a driver oncogene for APL. *PML-RARA* blocks myeloid differentiation and cooperates with a second mutation to induce aggressive leukemia^{48–50}. Similar to *PML-RARA*, the *CR* fusion itself is insufficient to induce advanced leukemia, suggesting that a second mutation is required to cooperate with the transformation. By analyzing the sequencing data from patient samples, we found frequently co-occurring mutations, including *NRAS*, *KRAS* and *WT1* mutations. However, no *FLT3-ITD* mutation was observed, which was proved to be the second hit in APL genesis^{48,51}. Indeed, both *NRAS*^{G12D} and *KRAS*^{Q61H} promoted the rapid transformation of *CR*-expressing HSPCs into leukemia cells. Our model is consistent with the two-hit theory and reveals the role of *CR* fusions in the development of myeloid malignancies.

RAR γ is a ligand-dependent transcriptional activator or repressor^{15,52}. It plays an essential role in chromatin remodeling in primitive hematopoietic precursors^{14,16}. The molecular mechanism of *CR* fusions in regulating transcription and how aberrant transcription contributes to disease development is unknown. To understand the distinctive trans-regulatory properties of *CR* fusions, we compared the DNA-binding abilities of the *CR* fusions with those of RAR γ . Notably, *CR* fusions exhibited a higher binding affinity for DNA loci than RAR γ . While RAR γ exhibited a relatively weaker binding signal, it may still engage with DNA at the loci associated with overlapping peaks of CRL and CRS. Additionally, we observed 67.5% of the genes regulated by *CR* fusions overlapping with those regulated by RAR γ , indicating an indispensable role for the RAR γ segment within the functionality of *CR* fusions.

RAR γ functions by recruiting coactivators or corepressors³⁶, which supports our finding that *CR* fusions can also interact with the corepressor HDAC3. Approximately 30% of the DNA-binding sites of the *CR* fusions were found to be co-occupied by HDAC3. The genes occupied by *CR*-HDAC3 display a globally suppressed expression and mainly involved in the regulation of myeloid cell differentiation. Inhibition of HDAC3 activity or *HDAC3* silencing results in the dissociation of *CR* fusions from DNA-binding sites, leading to the up-regulation of myeloid-related genes and restoration of myeloid differentiation. A notable change was observed in PU.1, a crucial TF for myeloid maturation that is frequently downregulated in AML^{53–55}. Ectopic expression of PU.1 in CD34-*CR* cells resulted in a reduction of the colony-forming capacity and induction of myeloid maturation. While knockdown of *PU.1* expression in HL60-*CR* and U937-*CR* cells alleviated apoptosis induced by HDAC inhibitors. These data suggest that the *CR*-HDAC3-PU.1 axis plays a crucial role in myeloid malignancy, providing evidence for future targeted therapy against *CR*-driven leukemia with HDACs inhibitors.

HDACs inhibitors are used in AML to reactivate genes that are epigenetically silenced by oncogenic fusion proteins³⁸. It has also been reported that HDACs inhibitors overcome ATRA resistance in patients with *PLZF-RARA* or *TBL1R-RARA* by disrupting their association with corepressors^{56,57}. Here, using the established *CR*/*NRAS*^{G12D} and *WT*/*NRAS*^{G12D} mouse models, we confirmed that HDAC inhibitors selectively induced differentiation and apoptosis of *CR* fusion-blasts in vitro and in vivo. HDAC inhibitors significantly prolonged the survival of *CR*/*NRAS*^{G12D} mice with promising efficacy over ATRA. Based on our data, with *CR* fusion as a representative, we have proposed a potential therapeutic strategy for APL-like myeloid leukemia with *RARG* fusions.

Given that all patients with *RARG* fusions who received ATRA or/and ATO therapy exhibited drug resistance, we sought to propose the possible explanations. In contrast to *PML-RAR α* , we found that *CR* fusions cannot be degraded by ATRA, ATO or the combination, which is one of the main manifestations of ATRA and ATO treatment of APL^{1,3}. In addition, it was reported that activated RAR γ can reduce retinoid levels by activating regulators of ATRA metabolism⁵⁸. These evidence may explain the adverse response to ATRA therapy in patients with *RARG* fusions.

Interestingly, our investigation revealed that only 10–14% of *CR* target genes overlapped with the target genes of *PML-RAR α* , potentially accounting for the different pathogenesis between these two diseases. The similarity in pre-leukemic phenotypes but distinct target genes of *CR* fusions and *PML-RAR α* may be attributed to several factors. Firstly, the *RARA* and *RARG* segments in the fusions play pivotal roles in their functionality while exhibiting diverse molecular and biological functions. RAR γ exerts dual roles of transcription repression and activation in HSCs maintenance^{14,16}. In contrast, RAR α orchestrates trans-activation upon ligand binding^{15,59}, and is predominantly involved in myeloid differentiation⁵². Additionally, it is crucial to consider the impact of the partner gene in the fusions. CPFS6 serves as a fundamental subunit of the mRNA polyA site recognition complex, which determines the 3' UTR length of mRNA and subsequently influences protein expression levels⁶⁰. The entirely distinct function of *CPFS6* from that of *PML*, contributing to the substantial disparity in target genes regulated by these two fusion proteins.

Importantly, in our studies, we observed increased sensitivities of *CR*-AML cells compared to cells expressing *PML-RARA*, indicating that the sensitivity to HDAC inhibitors in *CR*-AML may involve a distinct mechanism from that in APL. Our study has demonstrated that the *CR* repressed target genes are specific to *CR*-AML and distinct from target genes of APL. Inhibition or knockdown of HDAC3 significantly upregulates the expression of these genes. Notably, PU.1 expression, a key target of *CR*-HDAC3, was restored by HDAC3 shRNAs or inhibitors, specifically within *CR*-AML cells but not in AML cells with *PML-RAR α* fusion, indicating different molecular mechanisms of HDAC3 inhibitors in *CR*-AML and APL. Taken together, these findings may indicate a high sensitivity and specificity of *CR*-AML cells to HDAC inhibitors. The molecular mechanisms contributing to the distinct sensitivities to HDAC inhibitors between *CR*-AML and APL needs to be further studied in future work.

Methods

Ethical statement

Umbilical vein cord blood (CB) from anonymized healthy donors was purchased from Shanghai Cord Blood Bank (Shanghai, China) in accordance with local ethics procedures. Mobilized peripheral blood (PB) from healthy donors was provided by the Hematological BioBank in the First Affiliated Hospital of Soochow University. No age and sex was considered for the participating healthy donors since that information was not recorded. The study was approved by local medical ethical committees (2023-372), and all the healthy donors contributed voluntarily and were provided with an informed consent form, which states that they would not obtain any compensation. All animals were raised in specific pathogen-free conditions and in accordance with the guidelines approved by the Institutional Laboratory Animal Care and Use Committee of Soochow University. Experiments were approved by the Ethics Committee of the First Affiliated Hospital of Soochow University.

Mice

CRL and *CRS* floxed mice were generated by CRISPR/Cas9⁶¹. *Vav-Cre* mice were provided by Jinyong Wang (Guangzhou Institutes of Biomedicine and Health, Chinese Academy of Sciences). *LysM-Cre* mice were obtained from the Jackson Laboratory. All transgenic mouse lines were C57BL/6. CD45.1 mice were obtained from Vital River Laboratory (Beijing, China). C57BL/6 mice were purchased from SLAC Laboratory Animal Center (Shanghai, China). NCG mice were purchased from GemPharmatech (Nanjing, China). Mice were kept under controlled 12 h light/dark cycles in individually ventilated cages under specific pathogen-free conditions. Mice were kept at 23 °C and 50% humidity, with unlimited access to food and water. All animals in experiments were sex and age matched, and in accordance with the guidelines approved by the Institutional Laboratory Animal Care and Use Committee of Soochow University.

Human samples

Umbilical vein cord blood (CB) from anonymized healthy donors was purchased from Shanghai Cord Blood Bank (Shanghai, China) in accordance with local ethics procedures. Mobilized peripheral blood (PB) from healthy donors was obtained from the First Affiliated Hospital of Soochow University. The study was approved by local medical ethical committees, and all healthy donors gave written informed consent. Next-generation sequencing (NGS) data for *RARG* fusions were obtained from a previous study²⁶.

Primary cell culture

CD34⁺ enriched cells were obtained by Ficoll gradient centrifugation and magnetic-bead separation⁶². Purified human CD34⁺ cells were cultured⁶² and transduced with lentivirus in StemSpan SFEM II medium (Stem Cell Technology) supplemented with 50 ng/ml Fms-related tyrosine kinase 3 ligand (FLT3L), 50 ng/ml stem cell factor (SCF), 10 ng/ml thrombopoietin (TPO), and 10 ng/ml interleukin-6 (IL6) for 3 days (all cytokines were purchased from PeproTech). Subsequently, transduced cells were sorted using a FACSaria II (BD) or selected with geneticin and puromycin, followed by culture in StemSpan SFEM II medium supplemented with cytokines (SCF, TPO, FLT3L, IL-3, IL-6, each 10 ng/ml) to induce myeloid differentiation¹⁰.

Flow cytometry and magnetic-activated cell sorting (MACS)

BM cells were obtained by crushing femurs, tibias, sternums, and pelvic bones with Iscove's modified Dulbecco's medium (IMDM, Hyclone) supplemented with 1% bovine serum albumin (BSA). Spleens were dissociated by crushing followed by trituration. PB cells were collected via the retro-orbital plexus. All cell suspensions were filtered through a 70 µm cell strainer. Spleen cells and PB cells were treated with ACK solution (150 mM NH₄Cl, 1 mM KHCO₃, and 0.1 mM EDTA) at room temperature for 10 min to lyse red blood cells, followed by immediately washing in PBS. For flow cytometric analysis, whole BM cells and ACK treated spleen and PB cells were incubated with antibody staining at 4 °C for 30 min in the dark. The cells were stained with lineage-APC, IL7R-APC, sca-1-APC-Cy7, c-kit-BV605, CD34-BV421 and CD16/32-PE-Cy7 for myeloid progenitor cells; lineage-APC, sca-1-APC-Cy7, c-kit-PE-Cy7, CD150-BV421 and CD48-BV605 for stem cell populations. Lineage markers for HSCs and progenitors were CD3, B220, Gr1, Mac1 and Ter119. Analysis was performed using a NovoCyte Flow Cytometer (ACEA Biosciences), and data were analyzed using FlowJo software (TreeStar). For isolation of c-Kit⁺ cell populations, cells were stained with c-Kit-PE antibody followed by microbeads conjugated anti-PE secondary antibodies. Cells then were enriched according to instructions of Mouse CD117 Positive Selection Kit (Stem Cell Technology). For isolation of human CD34⁺ cell populations, cells were stained with CD34-biotin antibody followed by microbeads conjugated avidin. Cells then were enriched according to instructions of Human CD34 Pos Selection Kit II (Stem Cell Technology).

Lentiviral transduction

Flag-CRL, *flag-CRS*, *flag-RARG*, *NRAS*^{G12D} and *KRAS*^{Q61H} were cloned into PCDH-SFFV-IRES-EGFP plasmid, respectively. ShRNAs oligonucleotides for *HDAC3* and *PUL1* were cloned into pLKO.1-U6-NGFR plasmid. The oligonucleotide sequences were summarized in the Supplementary Data 2. For virus packaging, lentiviruses were packaged using calcium phosphate transfection reagent⁶². The Kasumi-1, HL60 and U937 cell lines were infected with lentivirus at a multiplicity of infection (MOI) of 10 for 18 h, and the enriched human CD34⁺ cells or purified mouse CD117⁺ cells by MACS were infected with lentivirus at an MOI of 100 for 6–12 h. Transduced cells were used for in vitro assays or transplantation.

Colony-forming and replating assays

The transduced human CD34⁺ cells were cultured in a H4435 methylcellulose medium (stem cell technology)⁶². Colonies were scored

under a microscope 13–14 days post plating. Replating was carried out by inoculating cells from primary cultures into fresh H4435 methylcellulose medium, and colony counting and replating were performed every 7 days. Assays of mononuclear cells (MNCs) from knock-in mice or transplanted recipients were performed in a M3434 methylcellulose medium (StemCell Technology) at a concentration of 5×10^4 cells per 35 mm dish, and colony morphology and counting were performed 10–12 days after plating.

Xenograft model

NCG mice were purchased and bred under pathogen-free conditions at the Laboratory Animal Center of Soochow University. The mice were then irradiated with 200 cGy of X-rays and subsequently injected with transduced human CD34⁺ cells at a dose of 2×10^5 through the tibia. At 10–12 weeks post transplantation⁶², BM cells of recipients were flushed down with IMDM supplemented with 1% BSA, followed by filtration through a 70 µm cell strainer. Then, the cells were treated with ACK solution for 10 min at room temperature. BM engraftment was assessed by flow cytometry. Cells were washed and stained with antibodies at 4 °C for 30 min in the dark. CD45-APC for total engraftment, CD34-PE-Cy7 and CD38-PE for stem/progenitor cells, CD19-PE for B cells, and CD33-APC and CD66b-BV421 for myeloid cells. Analysis was performed using a NovoCyte Flow Cytometer (ACEA Biosciences), and data were analyzed using FlowJo software (TreeStar).

Complete blood counts

Blood was collected via the retro-orbital plexus and complete blood counts were performed on an ADVIA 2120i (Siemens Healthineers) according to the manufacturer's protocol.

Competitive transplantation and the secondary transplantation

Recipient mice (45.1) received total body irradiation of 800 cGy (2 doses of 400 cGy with 4 h intervals) by an RAD 320 X-ray irradiator. Vav-CRL, Vav-CRS or WT BM cells were mixed with competitor (CD45.1) BM cells at a 1:1 ratio, and a total of 2×10^6 cells were transplanted into irradiated CD45.1 mice via retro-orbital injection. After transplantation, mice were maintained on antibiotic water for 4 weeks. Sixteen weeks post transplantation, the BM cells of the recipients were analyzed by flow cytometry⁶³. CD45.1-APC and CD45.2-APC-Cy7 for engraftment; Mac1, Gr1 and c-kit for myeloid cells and myeloid immature cells; lineage-APC, IL7R-APC, sca-1-APC-Cy7, c-kit-BV605, CD34-BV421 and CD16/32-PE-Cy7 for myeloid progenitor cells. For the secondary transplantation, a total of 2×10^6 BM cells from the first recipients of WT, Vav-CRL and Vav-CRS were transplanted into freshly irradiated CD45.1 mice (2 doses of 400 cGy with 4 h intervals) via retro-orbital injection. The BM cells of the recipients were analyzed by flow cytometry after 14–16 weeks.

Cytospin and histology

Cytospins of human CD34⁺ cells and BM cells from knock-in mice or transplanted recipients were stained with Wright-Giemsa. Tissue samples were fixed in formalin, dehydrated, and embedded in paraffin. Sectioned slides were rehydrated, followed by a standard hematoxylin and eosin (H&E) staining protocol. For immunohistochemistry (IHC), antigen was retrieved by boiling slides in 10 mmol/L sodium citrate buffer at 90–100 °C for 20 min and then cooled to room temperature. After washing twice with PBS, slides were incubated in 3% H₂O₂ for 25 min followed by blocking with BSA. The primary antibody used was myeloperoxidase (Abcam, #ab208670). Detection was performed with DAB Substrate (Beyotime), followed by hematoxylin counterstaining (Sigma-Aldrich). Myeloperoxidase stained BM sections were imaged, and the mean DAB intensity of staining was calculated using an open source bioimage software QuPath (v.0.2.3) according to the reported method⁶⁴.

Leukemic mouse model

C-kit⁺ cells of Vav-CRL, Vav-CRS or WT mice were isolated by magnetic-bead separation with a mouse CD117 positive selection kit (StemCell Technology) according to the manufacturer's protocols. The isolated c-kit⁺ cells were transduced with lentivirus expressing *NRAS*^{G12D}, *KRAS*^{Q61H} or empty vector. Subsequently, 2×10^5 transduced cells were transplanted into semilethally irradiated recipients (500 cGy) by tibial injection⁶⁵. The percentage of GFP⁺ cells was quantified by flow cytometry of periorbital blood, sampled at 2-week intervals. Ninety days post transplantation, viable cell numbers in the BM or spleen of recipients were determined with an automated cell counter (Countstar) by acridine orange/propidium iodide (AOPI) staining. Recipient BM and spleen cells were analyzed by flow cytometry. Mac1-PE-Cy7 and Gr1-BV421 for myeloid cells; Ter-119-APC for erythrocytes; B220-APC for B cells; and CD3-PE-Cy7 for T cells. The leukemia burden in the mice remained within the ethical committee's stipulated limits, which specified that the maximum allowable leukemia burden should not exceed 25% of circulating CD45⁺ cells or 80% of bone marrow CD45⁺ cells.

In vivo drug experiment

BM cells from CRL/N mice or WT/N mice were isolated, and 2×10^5 cells were transplanted into semilethally irradiated recipients (500 cGy) by retro-orbital injection. Five days post transplantation, mice were intraperitoneally injected once a day (QD) with vehicle (5% DMSO, 40% PEG300 and 10% Tween 80 in water) or all-trans retinoic acid (ATRA) at 10 mg/kg⁶⁶, or once every other day (QOD) with RGFP966 at 20 mg/kg⁴⁰, or tucidostat at 10 mg/kg⁴¹, for 15 days. ATRA, RGFP966 and tucidostat were purchased from SelleckChem and suspended in vehicle. After 20 days following the transplantation, leukemia burden is evaluated upon completion of the treatment regimen.

CUT&Tag-Seq and data analysis

The CUT&Tag assay was performed as described previously with modifications⁶⁶. Briefly, human CD34⁺ cells stably expressing flag-CRL, flag-CRS or flag-RAR γ were collected. CD34-CRL and CD34-CRS cells treated with 2 μ M RGFP966 or 0.1 μ M tucidostat for 9 days were collected. All the cells were immobilized on concanavalin A coated magnetic beads. Then, the cell membranes were permeabilized with digitonin. Next, the cells were incubated sequentially with flag (Sigma-Aldrich, #F1804), HDAC3 (Abcam, #ab32369), H3K27me3 (Diagenode, #C15410195) antibodies or normal mouse/rabbit IgG (Sigma-Aldrich), secondary antibodies, and PA-Tn5. DNA was purified using phenol-chloroform-isoamyl alcohol extraction and ethanol precipitation. Libraries were amplified using universal i5 and uniquely barcoded i7 primers. Sequencing was performed in the Illumina NovaSeq 6000 (Illumina) using 150 bp paired-end at Jiayin Biotechnology Ltd. (Shanghai, China). The bam file generated by the unique mapped reads was used as an input file, and macs2 software was used for callpeak with a cutoff *q*value < 0.05. The CUT&Tag-seq assay for PML-RAR α was performed in human CD34⁺ cells expressing flag-PML-RAR α using a flag antibody.

RNA-seq and data analysis

Human CD34⁺ cells transduced with Vec, flag-CRL, flag-CRS or flag-RARG were cultured in myeloid differentiation medium for 14 days, and then the cells were collected and high-throughput RNA-seq was performed by Illumina HiSeq 2500 (Illumina) at CapitalBio Corporation (Beijing, China). The normalized gene expression value and differentially expressed genes (DEGs) were both analyzed by using the R package DESeq2⁶⁷. Genes with a *P* value < 0.05 and fold changes ≥ 2 or fold changes ≤ -2 were recognized as DEGs between the two samples. Signature enrichment analysis of these DEGs was conducted using Metascape⁶⁸. Gene set enrichment analysis (GSEA) was performed by using GSEA software version 2.2.2.4, which uses predefined gene sets

from the Molecular Signatures Database (MSigDB v6.2). Preranked-GSEA was performed using GseaPreranked function. To evaluate the correlation between CR target genes and CR-AML specific gene signatures, we used RNA-seq data of 8 CR-AML and 113 non-CR AML from previously report²⁶. Ranked gene lists were generated by gene expression in CR-AML patients compared to non-CR AML patients.

Single-cell RNA-seq and analysis

For the scRNA-seq of CR knock-in mice, C-kit⁺ and Mac1⁺ BM cells from 1 year-old WT (*n* = 2), LysM-CRL (*n* = 2) or LysM-CRS (*n* = 2) mice were flow-sorted and mixed at a 1:1 ratio. For the scRNA-seq of leukemic mice, C-kit⁺ and Mac1⁺ BM cells were flow-sorted from WT/V (*n* = 2), WT/N (*n* = 2), CRL/V (*n* = 2), CRL/N (*n* = 2), CRS/V (*n* = 2) and CRS/N (*n* = 1) mice 90 days post-transplantation. Then, the sorted cells were mixed at a 1:1 ratio. Cells were loaded onto the Chromium single cell controller (10x Genomics) to generate single-cell gel beads in the emulsion according to the manufacturer's protocol. Captured cells were lysed and the released RNA was barcoded through reverse transcription in individual gel-bead-in-emulsions. ScRNA-seq libraries were constructed using the Single Cell 3' Library and Gel Bead Kit V3.1. High-throughput sequencing of the library was performed using the paired-end sequencing model of the Illumina NovaSeq6000 sequencer with a sequencing depth of at least 100,000 reads per cell with paired-end 150 bp (PE150) reading strategy (performed by CapitalBio Technology, Beijing).

Cell Ranger (3.0.0) was used to perform alignment, filtering, barcode and unique molecular identifier (UMI) counting to generate feature-barcode-UMI matrices. The cDNA insert was aligned to the GRCm38/mm10 reference genome and human *NRAS*. The Seurat (4.3.0) R tool kit⁶⁹ was used to perform quality control and unsupervised clustering. Cells whose gene number was less than 1000 and whose mitochondrial gene ratio was more than 10% were regarded as abnormal and filtered out. To reduce the batch effect of the samples, we performed data integration using the Harmony method⁷⁰. The top 3000 variable genes of scaled data were used for principal component analysis (PCA) to reduce dimensionality. Uniform manifold approximation and projection (UMAP) dimensionality reduction was performed by the "RunUMAP" function with default parameters using the first 30 Harmony components. The graph-based Louvain clustering and partitioned clusters were performed by using the "FindClusters" function with a resolution parameter equal to 0.6. Markers of each cluster were performed with the "FindAllMarkers" function setting a logFC threshold of 0.25 and a minimum percentage of cells expressing the gene greater than 25% in at least one of the compared clusters.

Clusters were annotated based on the expression of known marker genes, as depicted in Supplementary Fig. 2e (marker genes defining clusters from WT and CR knock-in mice) and Supplementary Fig. 4h (marker genes defining clusters from WT/V, WT/N, CR/V and CR/N recipients). Leukemic cells were defined based on the specific sequences disparities between human *NRAS* and mouse *Nras*. DEGs between distinct clusters were identified using the "FindMarkers" function of the Seurat package. GO and KEGG pathway enrichment analyses were based on clusterProfiler⁷¹ and visualized by the enrichplot package.

RNA isolation and reverse transcription quantification PCR

Total RNA was extracted using TRIzol reagent in accordance with the manufacturer's instructions and reverse transcribed. Reverse transcription quantification polymerase chain reaction (RT-qPCR) was also performed using TB Green Premix Ex Taq II (Takara) in accordance with the manufacturer's instructions. All experiments were performed in triplicate with an ABI QuantStudio 3 Real-time PCR System (Applied Biosystems). The primer sequences are summarized in the Supplementary Data 2. Differences in cDNA input were normalized to the *ACTB* expression levels.

Reporting summary

Further information on research design is available in the Nature Portfolio Reporting Summary linked to this article.

Data availability

All data generated or analyzed during this study are included in the Article and Supplementary Information, with Source Data provided alongside this paper. The raw data and processed data of RNA-seq, CUT&Tag-seq and scRNA-seq data have been deposited in the Gene Expression Omnibus (GEO) under the accession number GSE245030. The gene signatures for myeloid differentiation stages were derived from dataset GSE42519. ChIP-seq data of NB4 cells was acquired from GSE126720. CUT&Tag-seq data in human CD34⁺ cells expressing *PML-RARA* was obtained from GSE243438. The RNA-seq data of 8 *CR*-AML and 113 non-*CR* AML patients were sourced from the Genome Sequencing Archive of the China National Genomics Data Center (accession number [HRA003955](https://www.gdc.cn/record/HRA003955)), upon the authorization and consent of Jianyan Huang (the First Affiliated Hospital, Zhejiang University School of Medicine, Hangzhou, China. Email: huangjinyan@zju.edu.cn). Source data are provided with this paper.

Luciferase reporter assay

HEK-293T cells were cotransfected with 100 ng of pcDNA3.1-*CRL/CRS* plasmid or pcDNA3.1 empty vector in combination with 10 ng of pRL-SV40 renilla plasmid and 100 ng of pGL3-promoter-luciferase reporter constructs using FuGENE6 Transfection Reagent (Promega) according to the manufacturer's protocol. After transfection for 24 h, cells were treated with vehicle, 2 μ M ATRA, 2 μ M RGFP966 or 0.1 μ M tudinostat for 24 h. Subsequently, both firefly luciferase activity and renilla luciferase activity were detected with the BioTek Synergy HTX Multi-Mode Microplate Reader (Agilent) using the Dual-Luciferase Reporter Assay System (Promega) in accordance with the manufacturer's instructions. Firefly luciferase activity was normalized to Renilla luciferase activity to control the transfection efficiency.

Statistics & reproducibility

GraphPad Prism 8.0 was used for all figure production and statistical analysis. All the data are shown as the mean \pm SD and were analyzed by unpaired two-tailed Student's *t* test for two groups. Significance analysis of three or more groups was determined using repeated-measures ANOVA with Dunnett's or Tukey's multiple-comparisons tests. Overall survival (OS) was analyzed by using the Kaplan-Meier methodology and comparisons were performed by using the log-rank test. No statistical method was used to predetermine sample size. No data were excluded from the analyses. The experiments were not randomized. The Investigators were not blinded to allocation during experiments and outcome assessment. Statistical parameters for each experiment are indicated in the relevant figure legend.

References

1. de Thé, H., Pandolfi, P. P. & Chen, Z. Acute Promyelocytic Leukemia: A Paradigm for Oncoprotein-Targeted Cure. *Cancer Cell* **32**, 552–560 (2017).
2. Yilmaz, M., Kantarjian, H. & Ravandi, F. Acute promyelocytic leukemia current treatment algorithms. *Blood Cancer J.* **11**, 123 (2021).
3. de Thé, H. & Chen, Z. Acute promyelocytic leukaemia: novel insights into the mechanisms of cure. *Nat. Rev. Cancer* **10**, 775–783 (2010).
4. Dos Santos, G. A., Kats, L. & Pandolfi, P. P. Synergy against PML-RAR α : targeting transcription, proteolysis, differentiation, and self-renewal in acute promyelocytic leukemia. *J. Exp. Med.* **210**, 2793–2802 (2013).
5. Balasundaram, N. et al. Metabolic adaptation drives arsenic trioxide resistance in acute promyelocytic leukemia. *Blood Adv.* **6**, 652–663 (2022).
6. Shao, X. et al. Deneddylation of PML/RAR α reconstructs functional PML nuclear bodies via orchestrating phase separation to eradicate APL. *Cell Death Differ.* **29**, 1654–1668 (2022).
7. Zhao, J. et al. The genetics and clinical characteristics of children morphologically diagnosed as acute promyelocytic leukemia. *Leukemia* **33**, 1387–1399 (2019).
8. Wen, L. et al. Clinical and molecular features of acute promyelocytic leukemia with variant retinoid acid receptor fusions. *Haematologica* **104**, e195–e199 (2019).
9. Yao, L. et al. Identification of novel recurrent STAT3-RARA fusions in acute promyelocytic leukemia lacking t(15;17)(q22;q12)/PML-RARA. *Blood* **131**, 935–939 (2018).
10. Osumi, T., Tsujimoto, S. I., Tamura, M., Uchiyama, M. & Nakabayashi, K. Recurrent RARB Translocations in Acute Promyelocytic Leukemia Lacking RARA Translocation. *Cancer Res.* **78**, 4452–4458 (2018).
11. Geoffroy, M. C. & de Thé, H. Classic and Variants APLs, as Viewed from a Therapy Response. *Cancers* **12**, 967 (2020).
12. Guarnera, L. et al. Atypical Rearrangements in APL-Like Acute Myeloid Leukemias: Molecular Characterization and Prognosis. *Front Oncol.* **12**, 871590 (2022).
13. Zhang, X., Sun, J., Yu, W. & Jin, J. Current views on the genetic landscape and management of variant acute promyelocytic leukemia. *Biomark. Res.* **9**, 33 (2021).
14. Purton, L. E. et al. RAR gamma is critical for maintaining a balance between hematopoietic stem cell self-renewal and differentiation. *J. Exp. Med.* **203**, 1615–1615 (2006).
15. Geoffroy, M. C., Esnault, C. & de Thé, H. Retinoids in hematology: a timely revival? *Blood* **137**, 2429–2437 (2021).

16. Ghiaur, G. et al. Regulation of human hematopoietic stem cell self-renewal by the microenvironment's control of retinoic acid signaling. *Proc. Natl Acad. Sci. USA* **110**, 16121–16126 (2013).
17. Walkley, C. R. et al. A Microenvironment-Induced Myeloproliferative Syndrome Caused by Retinoic Acid Receptor γ Deficiency. *Cell* **129**, 1097–1110 (2007).
18. Liu, T. H. et al. Identification of novel recurrent CPSF6-RARG fusions in acute myeloid leukemia resembling acute promyelocytic leukemia. *Blood* **131**, 1870–1873 (2018).
19. Qin, Y. Z., Huang, X. J. & Zhu, H. H. Identification of a novel CPSF6-RARG fusion transcript in acute myeloid leukemia resembling acute promyelocytic leukemia. *Leukemia* **32**, 2285–2287 (2018).
20. Miller, C. A. et al. A case of acute myeloid leukemia with promyelocytic features characterized by expression of a novel RARG-CPSF6 fusion. *Blood Adv.* **2**, 1295–1299 (2018).
21. Wang, M. et al. Identification of a recurrent fusion NUP98-RARG in acute myeloid leukaemia resembling acute promyelocytic leukaemia. *Br. J. Haematol.* **197**, E73–E78 (2022).
22. Song, Y. et al. A short report of novel RARG-HNRNPM fusion gene in resembling acute promyelocytic leukemia. *Hematology* **27**, 518–522 (2022).
23. Li, J., Zhang, Y., Li, J., Xu, Y. & Zhang, G. A novel SART3::RARG fusion gene in acute myeloid leukemia with acute promyelocytic leukemia phenotype and differentiation escape to retinoic acid. *Haematologica* **108**, 627–632 (2023).
24. Wu, H. et al. Report of PRPF19 as a novel partner of RARG and the recurrence of interposition-type fusion in variant acute promyelocytic leukemia. *Hematol. Oncol.* **41**, 784–788 (2023).
25. Su, Z. et al. Novel reciprocal fusion genes involving HNRNPC and RARG in acute promyelocytic leukemia lacking RARA rearrangement. *Haematologica* **105**, e376–e378 (2020).
26. Zhu, H. H. et al. A global study for acute myeloid leukemia with RARG rearrangement. *Blood Adv.* **7**, 2972–2982 (2023).
27. Li, J. et al. CPSF6-RARG-positive acute myeloid leukaemia resembles acute promyelocytic leukaemia but is insensitive to retinoic acid and arsenic trioxide. *Pathology* **55**, 407–412 (2023).
28. Chen, X. et al. A novel NPM1-RARG-NPM1 chimeric fusion in acute myeloid leukaemia resembling acute promyelocytic leukaemia but resistant to all-trans retinoic acid and arsenic trioxide. *Br. J. Cancer* **120**, 1023–1025 (2019).
29. Zhang, Z. L. et al. Acute myeloid leukemia with a novel CPSF6-RARG variant is sensitive to homoharringtonine and cytarabine chemotherapy. *Am. J. Hematol.* **95**, E48–E51 (2020).
30. Han, X. et al. Acute myeloid leukemia with CPSF6-RARG fusion resembling acute promyelocytic leukemia with extramedullary infiltration. *Ther. Adv. Hematol.* **12**, 2040620720976984 (2021).
31. Such, E. et al. A novel NUP98/RARG gene fusion in acute myeloid leukemia resembling acute promyelocytic leukemia. *Blood* **117**, 242–245 (2011).
32. Tao, S. et al. Acute Myeloid Leukemia with NUP98-RARG Gene Fusion Similar to Acute Promyelocytic Leukemia: Case Report and Literature Review. *Onco Targets Ther.* **13**, 10559–10566 (2020).
33. Ding, W. et al. Case report: Identification of a novel HNRNPC::RARG fusion in acute promyelocytic leukemia lacking RARA rearrangement. *Front Oncol.* **12**, 1028651 (2022).
34. Ha, J. S. et al. Identification of a novel PML-RARG fusion in acute promyelocytic leukemia. *Leukemia* **31**, 1992–1995 (2017).
35. Helsen, C. & Claessens, F. Looking at nuclear receptors from a new angle. *Mol. Cell Endocrinol.* **382**, 97–106 (2014).
36. Cordeiro, T. N. et al. Interplay of Protein Disorder in Retinoic Acid Receptor Heterodimer and Its Corepressor Regulates Gene Expression. *Structure* **27**, 1270–1285.e1276 (2019).
37. Tan, Y. et al. A PML/RAR α direct target atlas redefines transcriptional deregulation in acute promyelocytic leukemia. *Blood* **137**, 1503–1516 (2021).
38. Zhang, J., Gao, X. & Yu, L. Roles of Histone Deacetylases in Acute Myeloid Leukemia With Fusion Proteins. *Front Oncol.* **11**, 741746 (2021).
39. Monticelli, S. & Natoli, G. Transcriptional determination and functional specificity of myeloid cells: making sense of diversity. *Nat. Rev. Immunol.* **17**, 595–607 (2017).
40. Dai, B. et al. Targeting HDAC3 to overcome the resistance to ATRA or arsenic in acute promyelocytic leukemia through ubiquitination and degradation of PML-RAR α . *Cell Death Differ.* **30**, 1320–1333 (2023).
41. Wang, H. et al. Chidamide increases the sensitivity of refractory or relapsed acute myeloid leukemia cells to anthracyclines via regulation of the HDAC3-AKT-P21-CDK2 signaling pathway. *J. Exp. Clin. Cancer Res.* **39**, 278 (2020).
42. Minucci, S. & Pelicci, P. G. Histone deacetylase inhibitors and the promise of epigenetic (and more) treatments for cancer. *Nat. Rev. Cancer* **6**, 38–51 (2006).
43. Matthews, G. M. et al. Functional-genetic dissection of HDAC dependencies in mouse lymphoid and myeloid malignancies. *Blood* **126**, 2392–2403 (2015).
44. Zhang, Y. et al. JAM3 maintains leukemia-initiating cell self-renewal through LRP5/AKT/ β -catenin/CCND1 signaling. *J. Clin. Invest* **128**, 1737–1751 (2018).
45. Ghyselinck, N. B. & Duester, G. Retinoic acid signaling pathways. *Development* **146**, dev167502 (2019).
46. Brown, G. Deregulation of All-Trans Retinoic Acid Signaling and Development in Cancer. *Int J. Mol. Sci.* **24**, 12089 (2023).
47. Brown, G. Targeting the Retinoic Acid Pathway to Eradicate Cancer Stem Cells. *Int J. Mol. Sci.* **24**, 2373 (2023).
48. Sohal, J. et al. A model of APL with FLT3 mutation is responsive to retinoic acid and a receptor tyrosine kinase inhibitor, SU11657. *Blood* **101**, 3188–3197 (2003).
49. Le Beau, M. M. et al. Recurring chromosomal abnormalities in leukemia in PML-RARA transgenic mice identify cooperating events and genetic pathways to acute promyelocytic leukemia. *Blood* **102**, 1072–1074 (2003).
50. Song, H. et al. Recurrent noncoding somatic and germline WT1 variants converge to disrupt MYB binding in acute promyelocytic leukemia. *Blood* **140**, 1132–1144 (2022).
51. Kelly, L. M. et al. PML/RAR α and FLT3-ITD induce an APL-like disease in a mouse model. *Proc. Natl. Acad. Sci. USA* **99**, 8283–8288 (2002).
52. Collins, S. J. The role of retinoids and retinoic acid receptors in normal hematopoiesis. *Leukemia* **16**, 1896–1905 (2002).
53. Wang, K. et al. PML/RAR α targets promoter regions containing PU.1 consensus and RARE half sites in acute promyelocytic leukemia. *Cancer cell* **17**, 186–197 (2010).
54. Rosenbauer, F. et al. Acute myeloid leukemia induced by graded reduction of a lineage-specific transcription factor, PU.1. *Nat. Genet.* **36**, 624–630 (2004).
55. Will, B. et al. Minimal PU.1 reduction induces a preleukemic state and promotes development of acute myeloid leukemia. *Nat. Med.* **21**, 1172–1181 (2015).
56. Li, S. et al. A novel fusion protein TBLR1-RAR α acts as an oncogene to induce murine promyelocytic leukemia: identification and treatment strategies. *Cell Death Dis.* **12**, 607 (2021).
57. He, L. Z. et al. Histone deacetylase inhibitors induce remission in transgenic models of therapy-resistant acute promyelocytic leukemia. *J. Clin. Invest* **108**, 1321–1330 (2001).
58. Hernandez, D. et al. Overcoming microenvironment-mediated protection from ATRA using CYP26-resistant retinoids. *Leukemia* **34**, 3077–3081 (2020).
59. Kashyap, V. et al. RAR γ is essential for retinoic acid induced chromatin remodeling and transcriptional activation in embryonic stem cells. *J. Cell Sci.* **126**, 999–1008 (2013).

60. de Prisco, N. et al. Alternative polyadenylation alters protein dosage by switching between intronic and 3'UTR sites. *Sci. Adv.* **9**, eade4814 (2023).
61. Platt, R. J. et al. CRISPR-Cas9 knockin mice for genome editing and cancer modeling. *Cell* **159**, 440–455 (2014).
62. Liu, T. H. et al. Expression of the fetal hematopoiesis regulator FEV indicates leukemias of prenatal origin. *Leukemia* **31**, 1079–1086 (2017).
63. Gu, Z. M. et al. Loss of EZH2 Reprograms BCAA Metabolism to Drive Leukemic Transformation. *Cancer Discov.* **9**, 1228–1247 (2019).
64. Rajakumar, S. A. et al. Targeted blockade of immune mechanisms inhibit B precursor acute lymphoblastic leukemia cell invasion of the central nervous system. *Cell Rep. Med.* **2**, 100470 (2021).
65. Zhang, M. et al. Functional, structural, and molecular characterizations of the leukemogenic driver MEF2D-HNRNPUL1 fusion. *Blood* **140**, 1390–1407 (2022).
66. Kaya-Okur, H. S. et al. CUT&Tag for efficient epigenomic profiling of small samples and single cells. *Nat. Commun.* **10**, 1930 (2019).
67. Robinson, M. D., McCarthy, D. J. & Smyth, G. K. edgeR: a Bioconductor package for differential expression analysis of digital gene expression data. *Bioinformatics* **26**, 139–140 (2010).
68. Zhou, Y. Y. et al. Metascape provides a biologist-oriented resource for the analysis of systems-level datasets. *Nat. Commun.* **10**, 1523 (2019).
69. Hao, Y. H. et al. Integrated analysis of multimodal single-cell data. *Cell* **184**, 3573–3587 (2021).
70. Korsunsky, I. et al. Fast, sensitive and accurate integration of single-cell data with Harmony. *Nat. Methods* **16**, 1289–1296 (2019).
71. Yu, G. C., Wang, L. G., Han, Y. Y. & He, Q. Y. clusterProfiler: an R Package for Comparing Biological Themes Among Gene Clusters. *OMICS* **16**, 284–287 (2012).

Acknowledgements

The authors thank Beijing Chao-Yang Hospital, first affiliated hospital of Nanchang University and Zhejiang University for providing the NGS data and RNA-seq data of CR-AML patients. We appreciate Ke Li for providing us blasts from the CR-AML patient-derived xenograft model. We thank Zhimin Gu, Meng Zhao and Peng Xu for helping to edit the manuscript. This work was supported by National Key Research and Development Program (2022YFC2502700) to Y.X., National Natural Science Foundation of China (82020108003 to D.W., 82070187 and 82370213 to Y.X.). T.L. was supported by Excellent Youth Science Fund of Jiangsu Province (BK20211553) and Translational Research Grant of NCRCH (2021ZKMB01), D.W. was supported by Priority Academic Program Development of Jiangsu Higher Education Institutions (PAPD) and Jiangsu Provincial Medical Innovation Center (CXZX202201).

Author contributions

Y.X. and T.L. designed the study, T.W. performed the experiments in human cells, L.Q., Y.L. and Y.F. performed animal experiments. L.Q. performed western blot and IP assays. Y.L. and S.L. performed the mice genotyping. M.S. helped to perform scRNA-seq and RNA-Seq analysis. F.W. helped to conduct the CUT&Tag-seq analysis. T.L. generated figures. D.W. and S.C. provided scientific guidance for the research. L.W. provided clinical samples. T.L. wrote the manuscript. Y.X., S.C. and D.W. jointly supervised this work.

Competing interests

The authors declare no competing interests.

Additional information

Supplementary information The online version contains supplementary material available at <https://doi.org/10.1038/s41467-024-54860-4>.

Correspondence and requests for materials should be addressed to Suning Chen, Depei Wu or Yang Xu.

Peer review information *Nature Communications* thanks Chi Wai Eric So, and the other, anonymous, reviewer(s) for their contribution to the peer review of this work. A peer review file is available.

Reprints and permissions information is available at <http://www.nature.com/reprints>

Publisher's note Springer Nature remains neutral with regard to jurisdictional claims in published maps and institutional affiliations.

Open Access This article is licensed under a Creative Commons Attribution-NonCommercial-NoDerivatives 4.0 International License, which permits any non-commercial use, sharing, distribution and reproduction in any medium or format, as long as you give appropriate credit to the original author(s) and the source, provide a link to the Creative Commons licence, and indicate if you modified the licensed material. You do not have permission under this licence to share adapted material derived from this article or parts of it. The images or other third party material in this article are included in the article's Creative Commons licence, unless indicated otherwise in a credit line to the material. If material is not included in the article's Creative Commons licence and your intended use is not permitted by statutory regulation or exceeds the permitted use, you will need to obtain permission directly from the copyright holder. To view a copy of this licence, visit <http://creativecommons.org/licenses/by-nc-nd/4.0/>.

© The Author(s) 2024